PROCEEDINGS OF SPIE

SPIEDigitalLibrary.org/conference-proceedings-of-spie

Three-dimensional surface capture for body measurement using projected sinusoidal patterns

Michelle H. Demers, Jeffery D. Hurley, Richard C. Wulpern, John R. Grindon

Michelle H. Demers, Jeffery D. Hurley, Richard C. Wulpern, John R. Grindon, "Three-dimensional surface capture for body measurement using projected sinusoidal patterns," Proc. SPIE 3023, Three-Dimensional Image Capture, (21 March 1997); doi: 10.1117/12.269760

SPIE.

Event: Electronic Imaging '97, 1997, San Jose, CA, United States

Three Dimensional Surface Capture for Body Measurement using Projected Sinusoidal Patterns

Michelle H. Demers, Jeffery D. Hurley, Richard C. Wulpern
Textile/Clothing Technology Corporation, Cary, North Carolina

John R. Grindon
John R. Grindon & Assoc.
Hazelwood, Missouri

ABSTRACT

A non-contact body measurement system (BMS) is under development for use in making made-to-measure apparel, and for other applications related to body measurement. The BMS design which consists of six stationary structured-light projectors and six CCD cameras is presented. The system acquires two-dimensional images of sinusoidal projected patterns utilizing a phase-shifting technique similar to phase measurement profilometry. Given calibrated projector and camera geometrical parameters, the solution for calculating three-dimensional surface points of a human body from the camera images is developed. A statistical error analysis is presented for the phase measurement and the three-dimensional point solution in terms of system measurement errors. An operating developmental implementation of the BMS is described and pictured. Contour plots of test subjects taken with this system, showing digitized three-dimensional surface segments, are presented and discussed.

Keywords: 3D image capture, 3D surface digitization, phase measurement profilometry, custom clothing, anthropometry

1. INTRODUCTION

The apparel industry, in order to be more competitive, is driving toward mass customization. This move toward made-to-measure apparel requires underlying technology to facilitate acquiring human body measurements and extracting appropriate critical measurements so that patterns can be altered for the customer. Traditionally, tailors have taken these measurements themselves for their own pattern altering methods. For this reason, tailors' measurements are notoriously inconsistent when compared with other tailors. An accurate data set of the surface of the body is needed in order to develop consistent body measurements.

Several technologies have been employed by researchers for body measurement including 2D video silhouette images, laser based scanning, and white light phase measurement. In order to get a full three-dimensional representation of the body without the use and cost of lasers, the white light phase measurement approach was chosen. Phase measurement profilometry (PMP) using structured white light was first introduced in 1986 by M. Halioua in Ref. 1. This approach required prior knowledge of the image field and continuity of the body surface. This paper presents an application of the PMP method with newly developed algorithms which resolve ambiguous surface discontinuities. Prior software calibration of the sensors is required.

The structured light and PMP application is well suited for body measurement because of the short acquisition time, accuracy and relatively low cost.

SPIE Vol. 3023 • 0277-786X/97/$10.00

2. BODY MEASUREMENT SYSTEM CONFIGURATION

2.1. System Design

The design of the BMS is based on unique coverage requirements of the human body. For example, in order to scan the majority of the population, the scanning volume was designed to be 1.1 m wide by 1.0 m thick by 2.0 m in height. From experiments on viewing the body from different angles, it was learned that more detail and coverage is required on the front surface of the body than on the back surface. For this reason, the BMS was designed with two front views with a 60 degree included angle and a straight on back view as shown in Figure 2.1. With this set of angles, there is overlap between views where detail is needed in high slope regions and minimal overlap on outer edge regions where surfaces are smooth. In order to get adequate height coverage, there are six views in total: three upper views and three lower views.

The system design uses six stationary surface sensors that encompass the body, rather than moving sensors or a moving body. This approach was selected because of the desire for a relatively short acquisition time, and moving sensors around a body or moving a body in front of a sensor in a few seconds presents dynamic issues. Since the sensors are stationary, each must capture an area segment of the surface, rather than a single contour on the surface. The area segments from the sensors are combined to form an integrated surface which covers at least those critical areas of the body that are needed for making apparel.

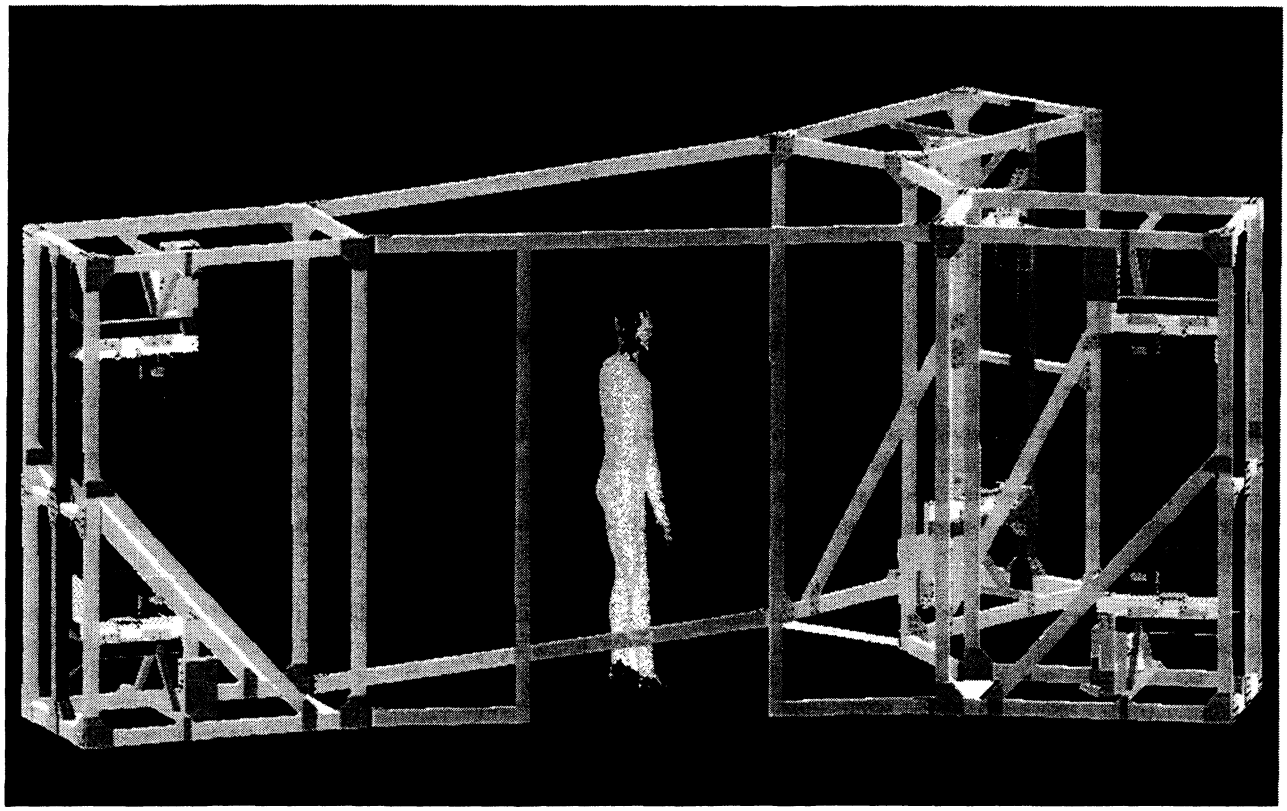

Figure 2.1 Mannequin positioned in the Body Measurement System for scanning.

2.2. Sensor Design

The structured light and PMP approach lends itself well to the area segment design. In this method, a sensor head, consisting of a projector and an area sensing camera, are paired together forming a vertical triangulation with the object or body as shown in Figure 2.2. The camera and projector are separated by a baseline to form the necessary geometry for mapping points onto the surface of the body. The projector contains a two-dimensional patterned grating which is projected

onto the body. The pattern varies in intensity sinusoidally in one direction, and is invariant in the perpendicular direction. Both coarse and fine grating patterns are employed. The projected pattern is imaged by an area array charge-coupled device (CCD) camera. See Figure 2.3.

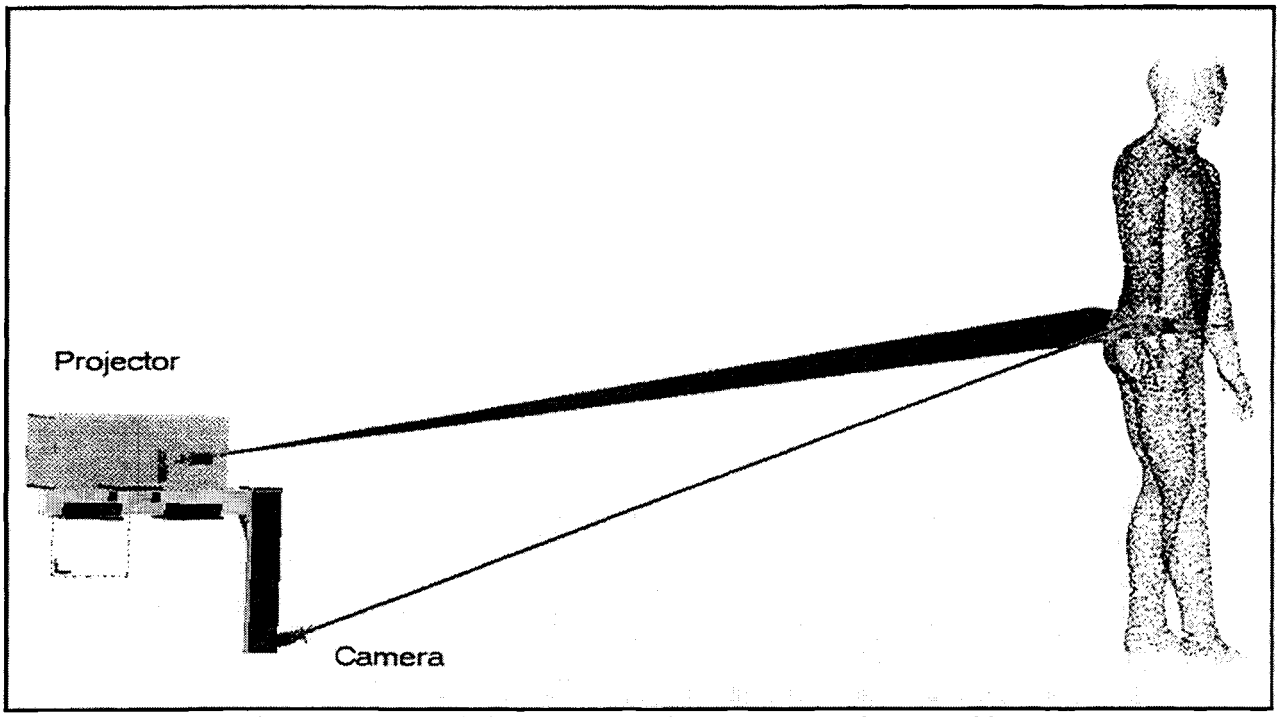

Figure 2.2 Triangulation between projector camera and target subject.

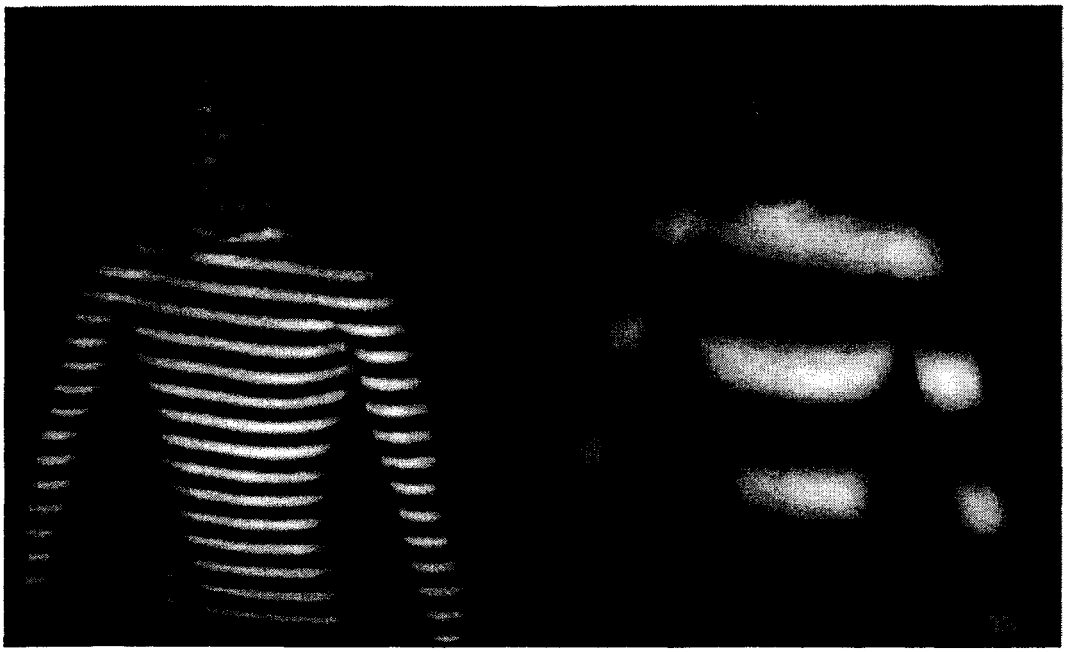

Figure 2.3 Sinusoidal patterns from fine and coarse grating projections.

2.3. System Hardware Design

The BMS structure is designed with an "erector set" approach in order to enable later adaptability to the changing needs of the development. The structure is built with black annodized aluminum extrusion and is covered with non-reflective black theater cloth for light tightness. The three viewing angles are achieved by arranging three pods as shown in Figure 2.1. Each pod contains two of the sensor heads described above to capture the full height of the body.

Each sensor head consists of an aluminum extrusion structure which rigidly holds a custom designed projector, commercial CCD camera and necessary controls for both. The cameras and projectors are controlled by a Pentium 133 personal computer. The computer contains 128 MB RAM, a motion control card, and two frame grabber boards. An additional electronics enclosure contains additional hardware and wiring necessary to interface the computer to the six sensor heads.

2.4. System Software Design

The software program was developed in the Microsoft Developer Studio Visual C++ under the Windows NT platform. OpenGL was utilized to create the graphics display tools. The software performs the following functions: graphical user interface, controlling the acquisition sequence, acquiring and storing image buffers, processing acquired images and calculating resulting data points, and displaying graphical output.

3. THEORY OF OPERATION

3.1. Phase Shifting

The PMP method involves shifting the grating preset distances in the direction of the varying phase and capturing images at each position. A total of four images is taken for each sensor, each with the same amount of phase shift, $\pi/2$ radians, of the projected sinusoidal pattern. Using the four images of the scene, the phase at each pixel can be determined. The basic PMP concept is described in Ref. 1. The advantage of the PMP method is that the phase value is independent of the ambient light level and the projector's light output. From Ref. 1, the general form of the projected pattern intensity is

$$I(x,y) = R(x,y)[A(x,y) + B(x,y)\cos(p(x,y))] \qquad (3.1.1)$$

where R(x,y) is the object reflectivity, A(x,y) represents the background intensity and B(x,y)/A(x,y) the fringe contrast. When four equal phase shifts of 90 degrees are acquired, the resultant phase function of the intensities in the ideal case is given by

$$p = \arctan\left[(I_4 - I_2) / (I_1 - I_3)\right] \qquad (3.1.2)$$

In the BMS, there are two sinusoidal gratings for each sensor, "fine" and "coarse". The fine grating has a 1 mm period and provides the required depth resolution of the data points. The coarse grating has a 5 mm period and provides gross depth information to resolve ambiguous phase data from the 1mm grating.

In the body measurement application, the pattern phases are shifted in steps of ninety degrees. The analytical model and the 3D solution is developed in Section 4 below. Accuracy is analyzed in Section 5.

3.2. Image Acquisition

Four images per sensor per grating are acquired. Since there are six sensors in the BMS, a total of 48 images are captured. In order to minimize the capture time, the computer acquires the images using a round robin acquisition scheme. In this manner, all of the images of the first grating position are captured in succession. After each sensor's image is acquired, the computer starts shifting the respective grating. When all six sensor images are acquired, the sequence is restarted for the next grating position. This process continues until all 24 images have been acquired for the 1mm grating. The gratings are then moved to project the 5 mm grating. The round robin sequence is repeated to acquire 24 images for the 5mm grating.

In this manner the critical portion of the scan, which occurs during the 1mm grating acquisition, is captured within 2 seconds.

4. THREE-DIMENSIONAL POINT SOLUTION

The phase information computed from the four images is used to calculate the three-dimensional data points. The calculated phase imaged by the pixel on the CCD array is used to determine a specific line of constant phase on the grating pattern. A schematic of the sensor head with the projected plane and camera ray is shown in Figure 4.1. The phase, p, is related to its spatial distance, x_p, on the grating by

$$(p + 2\pi \cdot m) = p_o + 2\pi \cdot r_g \cdot x_p \tag{4.1}$$

where p_o is the phase at x = 0, r_g is the spatial frequency of the sinusoidal pattern, and m is the 2π order with respect to x = 0. This line of constant phase, at a distance x_p, when projected through the nodal point of the projector lens, $q_{lp} = (x_{lp}, ylp, z_{lp})$, defines a unique plane in space. The equation of this plane is given by

$$\begin{bmatrix} z_{lp} & 0 & (x_p - x_{lp}) & -x_p z_{lp} \end{bmatrix} \begin{bmatrix} x \\ y \\ z \\ 1 \end{bmatrix} = 0 \tag{4.2}$$

A pixel location on the CCD array, q_{cc}, combined with the nodal point of the camera lens, q_{lc}, defines a unique ray in space.

$$\begin{bmatrix} x \\ y \\ z \\ 1 \end{bmatrix} = q_{cc} + k(q_{lc} - q_{cc}) \tag{4.3}$$

The parameter k traces points q_s along the ray.

$$q_s = q_{cc} + k(q_{lc} - q_{cc}) \tag{4.4}$$

The intersection of the plane projected from the projector and the ray from the CCD pixel defines the parameter k. Substituting k back into Eq. 4.2 yields the (x,y,z) location of the imaged surface.

$$k = -\frac{(z_{lp}x_{cc} + (x_p - x_{lp})z_{cc} - x_p z_{lp})}{(z_{lp}(x_{lc} - x_{cc}) + (x_p - x_{lp})(z_{lc} - z_{cc}))} \tag{4.5}$$

In Eq 4.1 all of the variables are known except the order m. The order is determined using the coarse 5 mm grating and the location of the scanning area. The 5 mm grating is coarse enough so that one cycle (0 to 2π) when projected would span the depth of the scanning area. For each ray from the CCD camera all the possible phases that would fall in the scanning area can be determined. The calculated phase from the four images can then be mapped onto the camera ray and its order is thereby determined. Once the order for the imaged phase on the coarse grating is determined, its x_p location is calculated on the grating. This x_p location is then used to resolve the order of the phase for the fine 1 mm grating. The x_p location on the grating that was determined from the coarse scan should be very close to the x_p location for the fine scan. The fine order is determined from the coarse x_p and the fine phase can be correctly mapped into this order assuming that the difference between the coarse scan and the fine scan is no greater than $\pm \pi$.

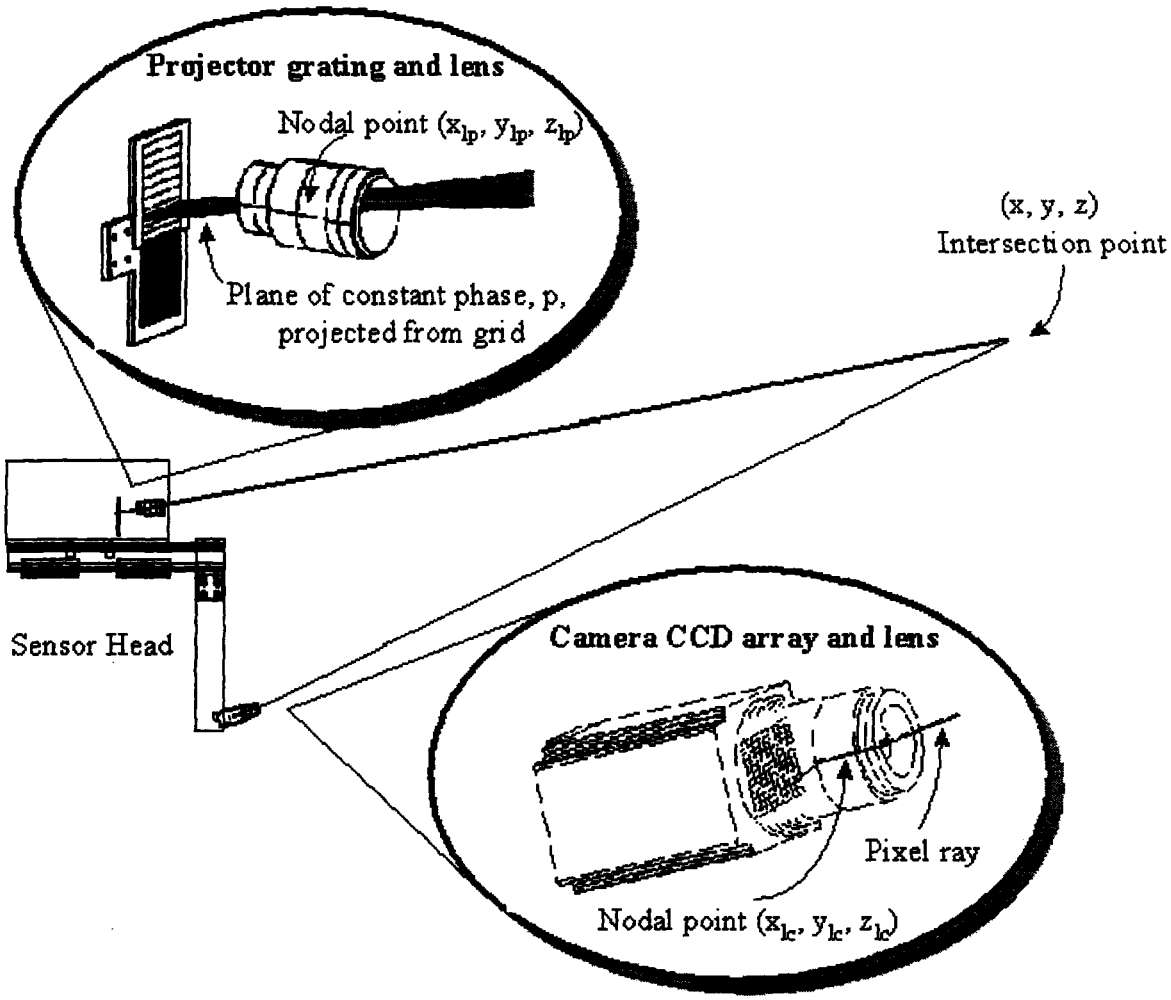

Figure 4.1 Schematic of sensor head with the projected plane and camera ray.

5. ANALYSIS OF PHASE MEASUREMENT AND DEPTH SOLUTION ERRORS

For a given sensor, one image is acquired for each of the four projected phase patterns. This was described in Section 3, preceding. The intensity values of these four images are processed at each pixel location to produce an estimate of the projected phase value at the corresponding imaged point on the subject. In contrast with edge-based pattern methods, such as that described in Ref. 2, the PMP method employs continuously varying amplitude patterns. The amplitude values convey the pattern information. Thus the 3D depth measurement accuracy depends upon the accuracy of measuring the image pixel values. The effect of image noise upon phase measurement accuracy is analyzed in Section 5.1. After systematic errors are removed, the remaining noise limits the achievable accuracy of phase measurement and the 3D depth solution. The analysis is continued in Section 5.2 to show the effect of phase measurement error upon 3D depth measurement accuracy.

5.1. Phase Error Standard Deviation Due To Image Noise

The phase measurement error standard deviation due to additive image noise is found. The noise is modeled as identically distributed, zero mean, uncorrelated random variables, n_1 through n_4 added to the respective image intensities, I_1 through I_4. Sources of this noise are quantization, granularity, and ensemble variations of the projected patterns themselves, as well as noise arising in the cameras and image acquisition system. The analysis makes use of the fact that the body measurement system is designed so that the noise standard deviation is small relative to the amplitude of the image signal.

Simplifying the notation of Eq. 3.1.1 without loss of generality, model the four image signals at a given pixel as

$$I_1 = a + b\cos(p) + n_1 \quad (5.1.1a)$$

$$I_2 = a + b\cos(p + \pi/2) + n_2 = a - b\sin(p) + n_2 \quad (5.1.1b)$$

$$I_3 = a + b\cos(p + \pi) + n_3 = a - b\cos(p) + n_3 \quad (5.1.1c)$$

$$I_4 = a + b\cos(p + 3\pi/2) + n_4 = a + b\sin(p) + n_4 \quad (5.1.1d)$$

Define

$$I_5 = (I_1 - I_3) / 2b = \cos(p) + n_5 \quad (5.1.1e)$$

$$I_6 = (I_4 - I_2) / 2b = \sin(p) + n_6 \quad (5.1.1f)$$

Where the random variables n_5 and n_6 are independent and identically distributed, given by

$$n_5 = (n_1 - n_3) / 2b \quad (5.1.2a)$$
$$n_6 = (n_4 - n_2) / 2b \quad (5.1.2b)$$

Estimate the phase p by p' where

$$p' = \arctan(I_6 / I_5) \quad (5.1.3)$$

For relatively low noise levels such as we expect, p' can be modeled by a first order expansion as follows:

$$p' = p + n_6\, \partial/\partial I_6 \arctan(I_6 / I_5) + n_5\, \partial/\partial I_5 \arctan(I_6 / I_5) \quad (5.1.4)$$

so the phase error, e, becomes

$$e = p' - p = (n_6 I_5 - n_5 I_6) / (I_5^2 + I_6^2) \quad (5.1.5)$$

But since

$$\cos^2(p) + \sin^2(p) = 1$$

we have, to the same first order approximation,

$$I_5^2 + I_6^2 = 1 \quad (5.1.6)$$

and

$$e = n_6\cos(p) - n_5\sin(p) \quad (5.1.7)$$

The variance is the statistically expected value of the (zero mean) error squared:

$$\text{var}(p) = E[e^2] = E[n_6^2\cos^2(p) - 2 n_5 n_6 \sin(p)\cos(p) + n_5^2\sin^2(p)] \quad (5.1.8)$$

Because the pattern noises have been reasonably taken to be statistically independent of the phase, zero mean, and statistically uncorrelated with one another, the expected value of the middle term is zero, and

$$var(p) = \cos^2(p)\, E[n_6^2] + \sin^2(p)\, E[n_5^2] \qquad (5.1.9)$$

and because they are identically distributed, with variance $var(n_0)$, it can be written that

$$\begin{aligned} E[n_6^2] &= E[n_5^2] \\ &= E[(n_1 - n_3)^2 / 4b^2] \\ &= (1 / 4b^2)\, E[n_1^2 - 2n_1 n_3 + n_3^2] \\ &= (1 / 4b^2)\ (E[n_1^2] + E[n_3^2]) \\ &= var(n_0) / 2b^2 \end{aligned} \qquad (5.1.10)$$

Thus the standard deviation of the phase error, std(p), is

$$std(p) = std(n_0) / (b \sqrt{2}), \quad b >> std(n_0) \qquad (5.1.11)$$

where std(p) is in radians. The sinusoidal pattern modulation amplitude, b, and the image noise standard deviation, $std(n_0)$, are in the same units. The value of b at a given pixel location in the image may be estimated as b' from the pixel values themselves, for the assumed low-noise condition using the relation

$$b' = ((I_1 - I_3)^2 + (I_2 - I_4)^2)^{1/2} / 2 \qquad (5.1.12)$$

Note that the phase error standard deviation varies inversely as the modulation amplitude b. Also, under the assumptions made, the phase error is independent of the phase value. This result is significant, for the phase error does not vary with the local slope of the sinusoidal pattern over the surface of the imaged subject. Thus the method described exhibits a well behaved response to image noise.

A signal to noise ratio, SNR, can be defined at a given pixel location as the ratio of the variance of the sinusoidal pattern signal component, $b^2 / 2$, to the noise variance, $var(n_0)$:

$$SNR = b^2 / (2\, var(n_0)) \qquad (5.1.13)$$

The phase error standard deviation can be expressed in terms of the SNR:

$$std(p) = 1 / (2 \sqrt{SNR}), \text{ rad}, \quad SNR >> 1 \qquad (5.1.14)$$

5.2. Depth Solution Error due to Phase Measurement Error

The effect of a phase measurement error is to produce an error in the solution for the target point position, or depth, along the ray defined by the camera lens nodal point and the modeled position of the pixel in 3D space. This is illustrated in Figure 5.1, which shows the relevant geometry projected onto an (x, y) plane. For analysis, the coordinates are defined as follows: the origin of the (x, y, z) coordinate system is defined at the projector lens nodal point, the x axis is defined to pass through the camera lens nodal point at x_c, and the (x, y) plane is defined to pass through the target point at (x_t, y_t).

The projector is modeled as a sinusoidal grating at an inclination angle of A with respect to the x axis, positioned at a perpendicular distance, (or focal length, f) from the lens nodal point. In practice, the grating is normally constructed to be invariant along one axis, and oriented so that the invariant axis is nominally parallel to the z axis as the coordinates are defined here. Thus in Figure 5.1, the invariant axis of the grating is perpendicular to the paper. The grating pattern varies sinusoidally along its length in the plane of the paper.

When a phase measurement is made, the solution model computes the distance, s, of the projected phase line along the grating from the point where a perpendicular line passes through the lens. If the pitch of the sinusoidal grating is r_g periods per millimeter, and the measured phase is p radians, then this distance is, in millimeters,

$$s = p / (2\pi r_g) \qquad (5.2.1)$$

The ray passing through the projector lens at the origin from the point at distance s along the grating -- which is in the (x, y) plane because for this analysis the target point is in the (x, y) plane -- defines a line at an angle P with respect to the x axis. This is shown in Figure 5.1.

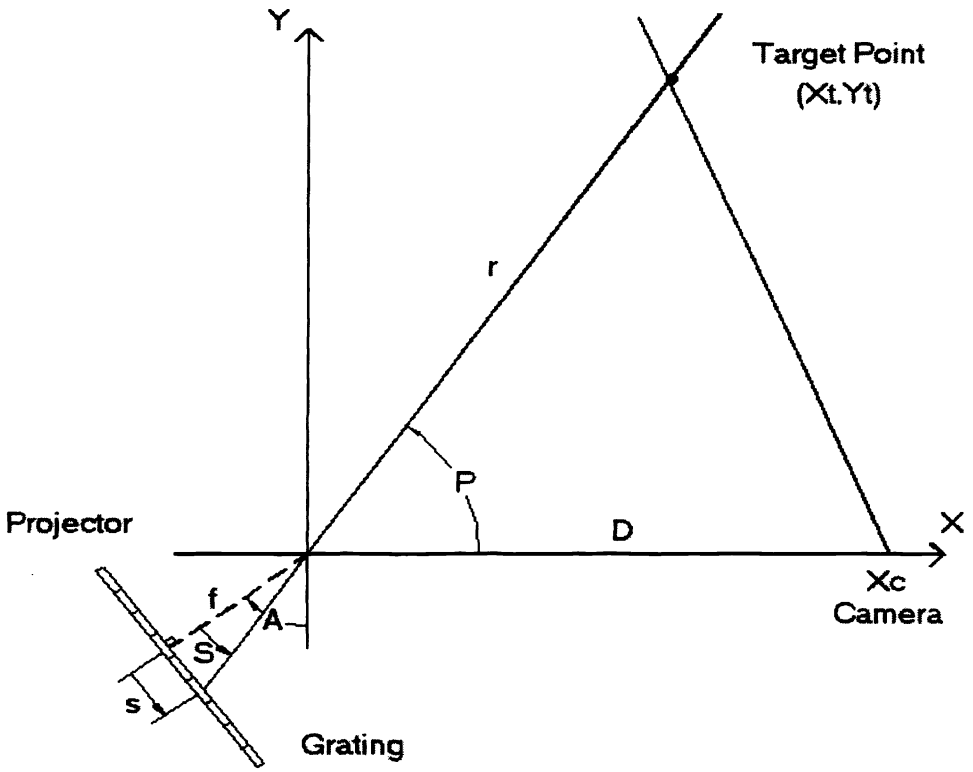

Figure 5.1 Depth Solution Geometry

An angle S is formed by this geometry, as illustrated in Figure 5.1, where

$$S = \arctan(s / f) \qquad (5.2.2)$$

The angle P is related to angles A and S by

$$P = S + A + \pi / 2 \qquad (5.2.3)$$

The effect of a phase measurement error, dp, is to produce an error dP in the solution for the angle P. First, define the projector constant c,

$$c = 2\pi f r_g \qquad (5.2.4)$$

Substituting first Eq. 5.2.1 and then Eq. 5.2.4 into Eq. 5.2.2, we have

$$S = \arctan(p/c) \qquad (5.2.5)$$

This constant has units of radians, and is a measure of the fineness of the projected pattern. The error in angle P caused by a phase measurement error dp is then, for small errors, found by taking the partial derivative of the angle P with respect to the phase p as follows

$$dP = (c / (c^2 + p^2)) dp \quad (5.2.6)$$

where the phase, p, can be expressed in terms of the angle P as

$$p = c \cot(A - P) \quad (5.2.7)$$

The standard deviation of the angle P is

$$std(P) = (c / (c^2 + p^2)) std(p) \quad (5.2.8)$$

We now have the error in angle P that is caused by a phase error dp. This is expressed in terms of the angle P, the grating inclination A, the projector lens focal length f, and the grating pitch in periods per millimeter, r_g. It remains to find the depth error along the camera ray.

Referring again to Figure 5.1, the ray through the projector lens is described by

$$y = x \tan(P) \quad (5.2.9)$$

and the ray through the camera lens by

$$y = y_t ((x - x_c) / (x_t - x_c)) \quad (5.2.10)$$

Defining r as the range from the projector lens to the target, using the substitutions in Eq's. 5.2.9 and 5.2.10,

$$x_t = r \cos(P) \qquad y_t = r \sin(P) \quad (5.2.11)$$

and taking partial derivatives, the x and y errors in the target point solution, dx and dy, produced by an angle error dP, are found to be, under the reasonable assumption of small errors,

$$dx = (r^2 (\cos(P) - x_c / r) / \; x_c \sin(P)) dP \quad (5.2.12)$$
$$dy = (r^2 / x_c) dP \quad (5.2.13)$$

Define D to be the baseline distance between the projector and the camera, i.e. $D = x_c$.

The standard deviation of the depth error is

$$std(depth) = std(P) (r^2/D) (1 + ((\cos(P) - D / r) / \sin(P))^2)^{1/2} \quad (5.2.14)$$

Note the r^2/D range dependence of depth error for $r >> D$. This is characteristic of triangulation-based depth measurement systems. For this analysis, the target point is defined to be in the (x, y) plane and the grating is taken to be aligned so that it is invariant with z. Thus the target point is centered, and no z-error is caused by an error in angle P. More generally, the target point will not be centered and there will be an error in z. In normal practice, the z error (perpendicular to the paper in Figure 5.1) is small compared to the depth error calculated using these equations.

6. DEVELOPMENTAL IMPLEMENTATION AND RESULTS

The intermediate output of the PMP process is a data cloud for each of the six views. See Figure 6.1. These data clouds must now be combined such that the resultant output is an accurate composite point cloud. The individual views are combined by knowing the exact orientation of each view with respect to one other. Their orientation is derived by calibrating the sensor heads in the system.

By scanning a calibration object of known size and orientation, we are able to calculate the orientation of each sensor head with respect to the object. By placing the calibration object approximately where the subject will be standing, we also have a coarse correlation between the object and the subject to be scanned. This is important not only to assure correct coverage but to make sure the subject is within the depth of focus of each of the sensor heads. During system calibration, the calibration

object is acquired using the acquisition sequence described in Section 3.2. Once the images have been acquired, they are processed and the resulting data points are determined with these data points being maintained in sensor head coordinates. Again, these data points may be seen in Figure 6.1. The system calibration process takes the area segment that is visible to each sensor and matches it to the calibration object using a minimization routine. Once the orientation of each sensor head has been determined, a transformation matrix is developed to transform the data into global coordinates. Figure 6.2 shows the resultant composite data set of a mannequin that was scanned with the BMS system. These data points are the raw calculated points without any smoothing or other post-processing.

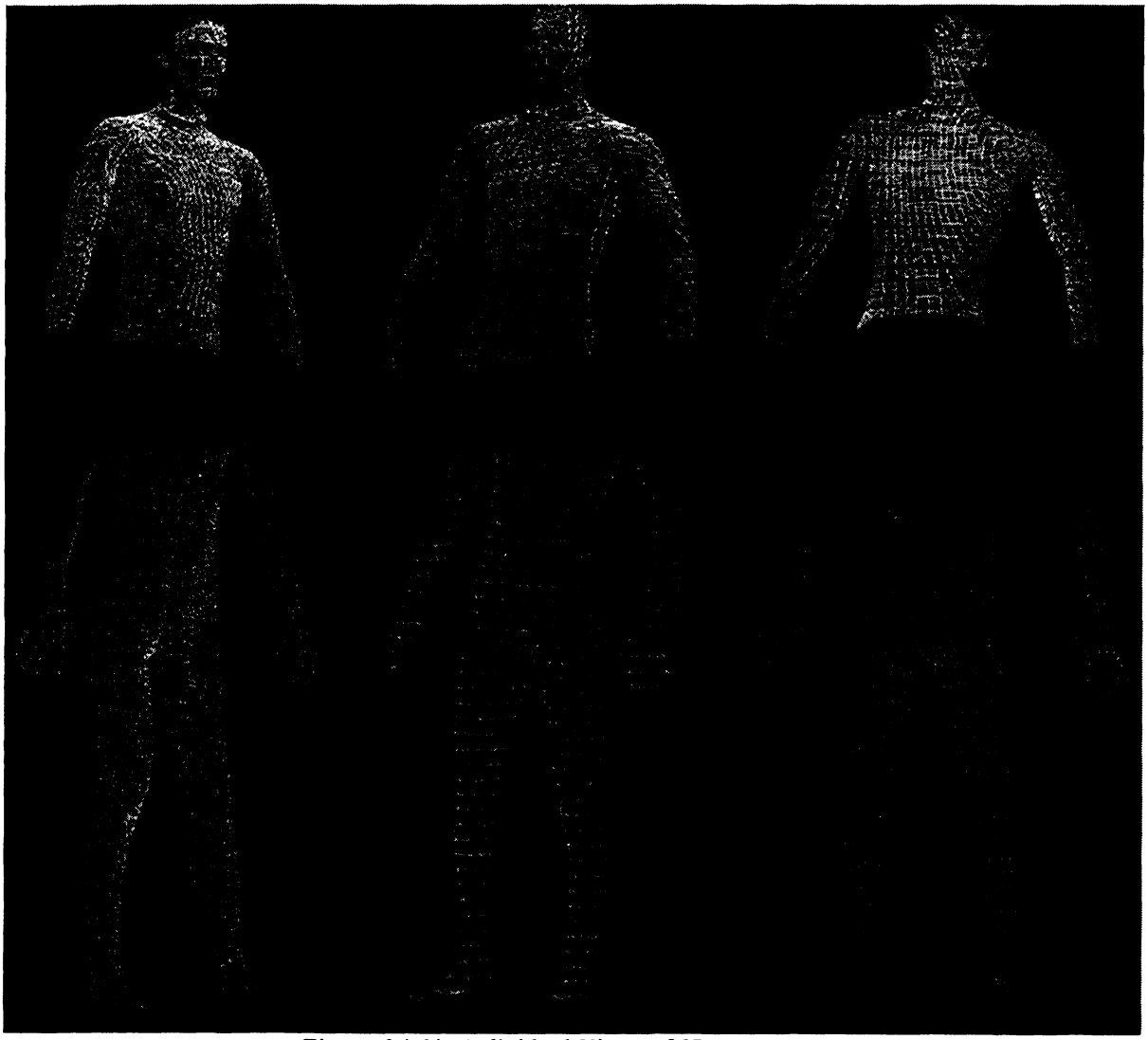

Figure 6.1 Six Individual Views of 3D Data Points

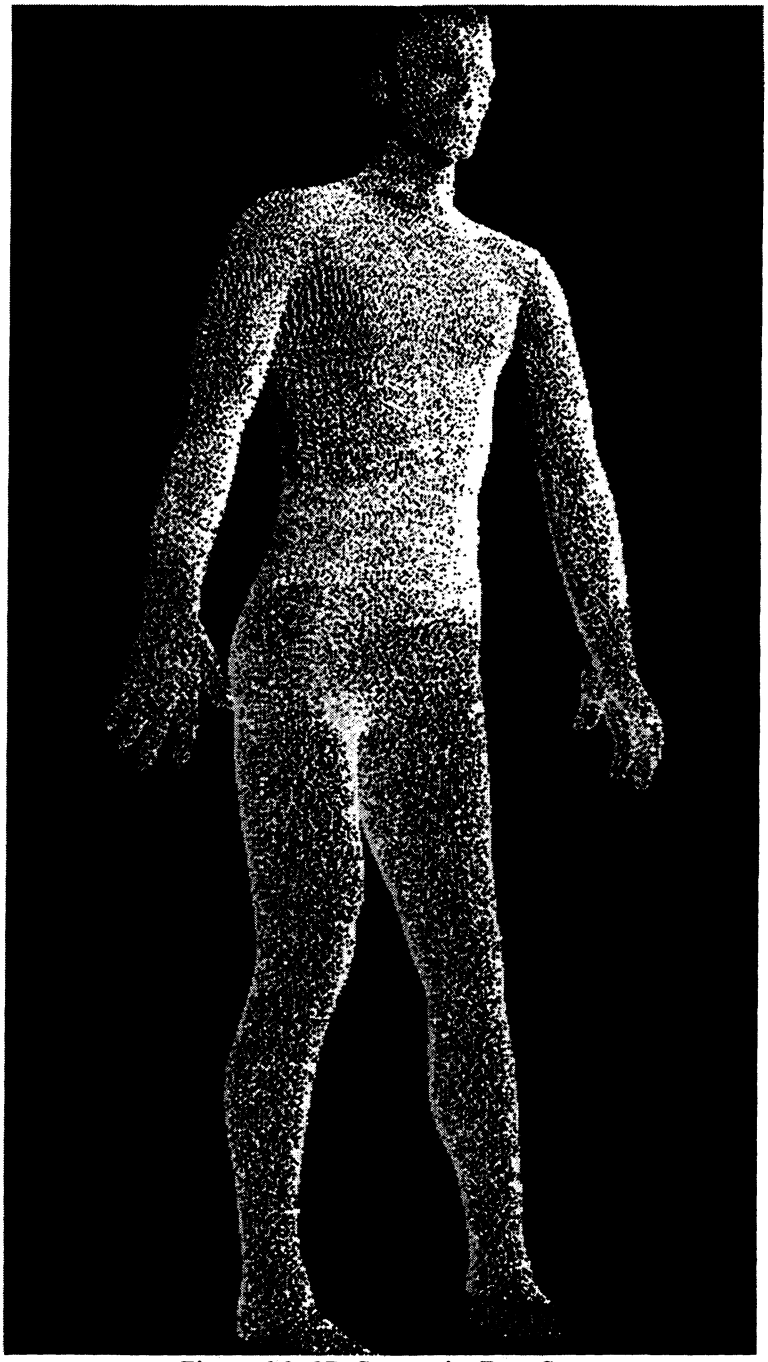

Figure 6.2 3D Composite Data Set

7. CONCLUSION

By close examination of the composite data set, it can be shown that good matching exists between the six views in the overlap regions. This is an indication that the system calibration is orienting the views properly and that the individual views are properly calibrated. Further verification of the calibration systems and refinement of the algorithms is continuing. Work is also progressing to extract tailor measurements from the body data sets and to alter garment patterns for making custom apparel.

ACKNOWLEDGEMENTS

This work was funded under a grant from the United States Department of Commerce.

REFERENCES

1. Halioua, M., L. Hsin-Chu, "Optical Three-Dimensional Sensing by Phase Measuring Profilometry", Optics and Lasers in Engineering, 0143-8166, pp.185-215, 1989.
2. Grindon, J. R., "Non-contact 3-D Surface Digitization of the Human Head", Proceedings of the National Computer Graphics Association Annual Conference, Atlanta, April, 1989.